Lattice Boltzmann and spectral simulations of non-linear stability of Kolmogoroff flows

C. TREVIÑO
Facultad de Ciencias, Universidad Nacional Autónoma de México
04510 México D.F., México

AND

F. HIGUERA
E.T.S.I. Aeronáuticos, U.P.M.
Plaza del Cardenal Cisneros 3, Madrid 28040 Spain

Recibido el 17 de enero de 1994; aceptado el 19 de septiembre de 1994

ABSTRACT. The non-linear stability of the Kolmogoroff flow is numerically studied using both spectral and lattice Boltzmann simulations with the aim of validating these latter techniques. Three different methods were applied: one standard spectral method and two types of lattice Boltzmann simulations. Results, in the form of streamline and vorticity patterns, are presented for different Reynolds and wave numbers (aspect ratio), showing generally good agreement among the three techniques and with well known results in the literature. This agreement is better for steady or quasi-steady situations, and an explanation for this feature is provided.

RESUMEN. En este trabajo se estudia numéricamente la estabilidad del flujo de Kolmogoroff empleando técnicas espectrales y red de malla de Boltzmann, con la finalidad principal de validar estas últimas técnicas. Se emplearon tres diferentes métodos: un método espectral y dos tipos de simulación con redes de malla. Se presentan resultados de patrones de función de corriente y vorticidad para diferentes números de Reynolds y de onda (relación de aspecto), mostrando en general buena concordancia entre las tres técnicas y con resultados ya establecidos en la literatura. La concordancia es mejor para flujo estacionario o cuasi-estacionario, para lo cual se da una explicación en este trabajo.

PACS: 47.20.Ft; 47.20.Ky; 47.30.+s

1. INTRODUCTION

The Kolmogoroff flow is called such a flow obtained for a viscous incompressible fluid induced by an unidirectional external force field periodic in one coordinate [1–3]. The study of this type of flow has received considerable attention in the past years due to the fact that is suitable to study large scale perturbations induced by viscosity driven at small scales [3]. The linear stability analysis was carried out by Meshalkin and Sinai [4] and independently by Green [5]. The marginal stability curve shows that the critical Reynolds number decreases with the perturbations' wave number, reaching the value of $\sqrt{2}$ for the wave number zero. This critical Reynolds number tends to infinity as the wave number of 1 is achieved (this corresponds to an aspect ratio of unity, same wave number as that given by the driving force). Beaumont [6] and Gotoh *et al.* [7] used Floquet theory after

taking into account modes which do not have the same periodicity as the unperturbed flow in the transversal direction.

Bondarenko *et al.* [8] have reproduced this type of flow in laboratory scale using a thin layer of electrolyte placed in a periodic magnetic field. He obtained a critical Reynolds number several orders of magnitude larger than $\sqrt{2}$, difference based on the different boundary conditions used in the experiment. They obtained for the Reynolds number three times larger than the critical one, irregular oscillations showing the appearance of turbulence, but the sequences of events leading to this state depend on the degree of confinement. Obukhov [3] analysed the model including friction and Thess [9] carried out a comprehensive linear stability analysis taking into account viscosity, linear friction and confinement. Thess found that strong confinement leads to oscillation at the onset of instability, contrary to the purely exponential grow obtained for weakly confined systems.

Sivashinsky [10], studied the non-linear bifurcation of this flow close to the critical value of $\sqrt{2}$, obtaining the evolution equation, which shows chaotic behavior (turbulence). The first bifurcation shows the existence of vortical periodic flows, the number of which depends on the Reynolds number and the wave number of the perturbation. It can be shown that these periodic flows are unstable, leaving only one vortical flow. She [11,12] constructed a simplified model and performed extensive numerical simulations of the non-linear evolution of the Kolmogoroff flow. Perturbed in the unstable band of the wave numbers, this flow reorganizes itself into a periodic or quasi-periodic array of vortices roughly aligned with the direction of the force. This is a relatively rapid process occurring in times of the order of the eddy turnover time, resulting in a variety of states depending very much in the initial perturbation. Later on, these sates, which are unstable to the pairing of two neighbor vortices, evolve by sequences of pairing events spaced by increasingly long time intervals of very little activity. The number of vortices decreases by one in each pairing and the overall length scale of the flow (in the direction of the force) increases accordingly. Numerical computations were extended up to about 10^3 eddy turnover times. Recently, Martínez *et al.* [13] made a comparison of spectral method and lattice Botzmann simulations on a two dimensional shear layer initial value spatially-periodic problem perturbed with a low level random noise. They found both simulations to be very close to each other in the history of enstrophy, wave number energy spectra and vorticity plots at least for times of the order of several turn-over times. They detected however discrepancies in the spatial position of vortical structures.

In this paper we present a numerical description of a part of the non-linear response of the Kolmogoroff flow to relatively short wavelength perturbations by two different numerical techniques: spectral (S) and lattice Boltzmann simulation (LB). The work is intended as an assessment of two variations of the lattice Boltzmann method which uses simplified versions of the lattice Boltzmann equation.

2. FORMULATION

We assume a two dimensional flow given by a velocity vector $\mathbf{v}^*(x,y)$, induced by a periodic gravity force in the x direction but modulated along the y coordinate. In terms of the vorticity, $\omega^* = \nabla^* \times \mathbf{v}^*$ ($\nabla^* = \mathbf{i}\partial/\partial x + \mathbf{j}\partial/\partial y$), and the stream function, ψ^*, defined

by $\partial\psi^*/\partial y = \mathbf{v}^* \cdot \mathbf{i}$ and $\partial\psi^*/\partial x = -\mathbf{v}^* \cdot \mathbf{j}$, the Navier-Stokes governing equations for this flow, called Kolmogoroff flow, can be written as

$$\frac{\partial\boldsymbol{\omega}^*}{\partial t} + \frac{\partial\psi^*}{\partial y}\frac{\partial\boldsymbol{\omega}^*}{\partial x} - \frac{\partial\psi^*}{\partial x}\frac{\partial\boldsymbol{\omega}^*}{\partial y} = \nu\left(\frac{\partial^2\boldsymbol{\omega}^*}{\partial x^2} + \frac{\partial^2\boldsymbol{\omega}^*}{\partial y^2}\right) + \frac{1}{\rho^*}\nabla^* \times \mathbf{f}^*, \tag{1}$$

$$\boldsymbol{\omega}^* = \left(\frac{\partial^2\psi^*}{\partial x^2} + \frac{\partial^2\psi^*}{\partial y^2}\right)\mathbf{k}, \tag{2}$$

where $\mathbf{f}^* = -F_0^* \sin(\pi y/h)\mathbf{i}$ denotes the body force and F_0^* its amplitude. The force is modulated along the y coordinate and directed in the direction of the x coordinate; h corresponds to the half wavelength of this modulation; $\mathbf{i}, \mathbf{j}, \mathbf{k}$ are the unit vectors corresponding to the x, y and z coordinates, respectively; t corresponds to the time; ν is the kinematic viscosity and ρ^* the density of the fluid. The stream function, ψ_{ss}^*, and vorticity, $\boldsymbol{\omega}_{ss}^*$, for the steady-state flow are given by

$$\psi_{ss}^* = -\frac{F_0^* h^3}{\mu\pi^2}\cos\left(\frac{\pi y}{h}\right), \tag{3}$$

$$\boldsymbol{\omega}_{ss}^* = \frac{F_0^* h}{\mu\pi}\cos\left(\frac{\pi y}{h}\right)\mathbf{k}. \tag{4}$$

Here, μ corresponds to the dynamic viscosity, $\mu = \rho^*\nu$. The longitudinal x-velocity component for the steady-state Kolmogoroff flow, is then

$$u_{ss}^* = \frac{F_0^* h^2}{\mu\pi^2}\sin\left(\frac{\pi y}{h}\right). \tag{5}$$

Introducing the following non-dimensional normalized variables:

$$\boldsymbol{\omega} = \boldsymbol{\omega}^* \frac{\mu\pi}{F_0^* h}; \qquad \psi = \psi^* \frac{\mu\pi^2}{F_0^* h^3}; \qquad \mathbf{f} = \frac{\mathbf{f}^*}{F_0^*},$$

$$\chi = \frac{x}{ah}; \qquad \eta = \frac{y}{h}; \qquad \tau = \frac{F_0^* t}{\mu\pi^2},$$

where a represents the aspect ratio L/h, the non-dimensional governing equations transform to

$$\frac{\partial\boldsymbol{\omega}}{\partial\tau} + \frac{1}{a}\frac{\partial\psi}{\partial\eta}\frac{\partial\boldsymbol{\omega}}{\partial\chi} - \frac{1}{a}\frac{\partial\psi}{\partial\chi}\frac{\partial\boldsymbol{\omega}}{\partial\eta} = \frac{1}{R}\nabla^2\boldsymbol{\omega} + \frac{\pi^2}{R}\cos(\pi\eta)\mathbf{k}, \tag{6}$$

$$\pi^2\boldsymbol{\omega} = \nabla^2\psi\mathbf{k}. \tag{7}$$

R corresponds to the Reynolds number defined with the maximum steady-state longitudinal velocity and is given by

$$R = \frac{F_0^* \rho h^3}{\pi^2 \mu^2} = \frac{u_m \rho h}{\mu}. \tag{8}$$

The non-dimensional Laplacian transforms to

$$\nabla^2 = \frac{1}{a^2}\frac{\partial^2}{\partial \chi^2} + \frac{\partial^2}{\partial \eta^2}.$$

An alternative form of the non-dimensional Navier-Stokes equations for the Kolmogoroff flow given by Eqs. (6) and (7) and preferable for the spectral numerical technique, because it conserves the kinetic energy in the inviscid limit, is the following:

$$\frac{\partial \mathbf{v}}{\partial \tau} = \frac{1}{R}\nabla^2 \mathbf{v} + \frac{\pi^2}{R}\mathbf{f} + \mathbf{v} \times \nabla \times \mathbf{v} - \nabla \Pi, \tag{9}$$

$$\nabla \cdot \mathbf{v} = 0, \tag{10}$$

where

$$\Pi = p + |\mathbf{v}^2|. \tag{11}$$

Equations (9) and (10) are to be solved with suitable initial conditions and the periodicity conditions

$$\mathbf{v}(0, \eta) = \mathbf{v}(1, \eta); \qquad \mathbf{v}(\chi, 0) = \mathbf{v}(\chi, 1), \tag{12}$$

$$\Pi(0, \eta) = \Pi(1, \eta); \qquad \Pi(\chi, 0) = \Pi(\chi, 1). \tag{13}$$

In the following sections we describe both the spectral and lattice Boltzmann methods used to solve this problem.

3. SPECTRAL METHOD

In this section we describe the spectral numerical technique to solve the governing equations, based in the Fourier Galerkin method. We introduce the discrete Fourier transform for all variables in the form

$$\mathbf{v}(\chi, \eta, \tau) = \sum_{m=-M}^{M} \sum_{n=-N}^{N} \mathbf{V}_{mn}(\tau) \exp(in\pi\eta + im\pi\chi). \tag{14}$$

The numerical calculation is performed by using a standard splitting technique described elsewhere [14,15]. In the first step, both the non-linear and body force terms are taken into account, that is

$$\frac{\partial \mathbf{v}}{\partial \tau} = \frac{\pi^2}{R}\mathbf{f} + \mathbf{v} \times \nabla \times \mathbf{v}. \tag{15}$$

Denoting by $\mathbf{G}_{mn}$ the Fourier transform of the right hand side of Eq. (15),

$$\mathbf{G}_{mn} = \int_{-1}^{1}\int_{-1}^{1} \left(\frac{\pi^2}{R}\mathbf{f} + \mathbf{v} \times \nabla \times \mathbf{v}\right) \exp(-in\pi\eta - im\pi\chi)\, d\eta\, d\chi, \tag{16}$$

and using the Adams-Bashforth discretization procedure, Eq. (15) takes the form

$$\mathbf{V}_1^{\tau+\Delta\tau} - \mathbf{V}^{\tau} = \Delta\tau\left(\tfrac{3}{2}\mathbf{G}^{\tau} - \tfrac{1}{2}\mathbf{G}^{\tau-\Delta\tau}\right), \tag{17}$$

where $\mathbf{V}_1^{\tau+\Delta\tau}$ corresponds to the discrete Fourier transform of the intermediate velocity vector at the new time $\tau + \Delta\tau$ and $\mathbf{V}^{\tau}$ is the true velocity vector at time τ. The Fourier transform in Eq. (16) is computed with the aid of the FFT algorithm. Aliasing is removed by using the 3/2 rule [15]. The time step $\Delta\tau$ used in the numerical integration is determined by the CFL stability condition. Using both velocity components, Eq. (17) takes the form

$$U_1^{\tau+\Delta\tau} - U^{\tau} = \Delta\tau\left(\tfrac{3}{2}G_{\chi}^{\tau} - \tfrac{1}{2}G_{\chi}^{\tau-\Delta\tau}\right),$$
$$V_1^{\tau+\Delta\tau} - V^{\tau} = \Delta\tau\left(\tfrac{3}{2}G_{\eta}^{\tau} - \tfrac{1}{2}G_{\eta}^{\tau-\Delta\tau}\right),$$

where G_{χ} and G_{η} are the corresponding components of the vector $\mathbf{G}$. The second step takes into account the total pressure term as well as the continuity equation. That is

$$\mathbf{V}_2^{\tau+\Delta\tau} - \mathbf{V}_1^{\tau+\Delta\tau} = -\Delta\tau\,\nabla\Pi_2^{\tau+\nabla\tau} \quad \text{and} \quad \nabla \cdot \mathbf{V}_2^{\tau+\Delta\tau} = 0. \tag{18}$$

These equations can be written in the following form:

$$U_2^{\tau+\Delta\tau} = U_1^{\tau+\Delta\tau} - \frac{im\pi\Delta\tau}{a}\Pi_2^{\tau+\nabla\tau},$$
$$V_2^{\tau+\Delta\tau} = V_1^{\tau+\Delta\tau} - in\pi\Delta\tau\,\Pi_2^{\tau+\nabla\tau},$$
$$\frac{m}{a}U_2^{\tau+\Delta\tau} + nV_2^{\tau+\Delta\tau} = 0.$$

Using the above relationships, Eqs. (18) then transform to

$$V_2^{\tau+\Delta\tau} = \frac{\left(\frac{m^2}{a^2}\right)V_1^{\tau+\Delta\tau} - \left(\frac{m}{a}\right)U_1^{\tau+\Delta\tau}}{1+\left(\frac{m^2}{a^2}\right)},$$

$$U_2^{\tau+\Delta\tau} = -\frac{an}{m}V_2^{\tau+\Delta\tau},$$

$$\Pi_2^{\tau+\Delta\tau} = \frac{i}{n\pi\Delta\tau}\left(V_2^{\tau+\Delta\tau} - V_1^{\tau+\Delta\tau}\right).$$

In the third and last step, the viscous term is considered in the form

$$\frac{\partial \mathbf{V}}{\partial \tau} = \frac{1}{R}\nabla^2\mathbf{V}.$$

Therefore, using an implicit scheme we obtain finally

$$U^{\tau+\Delta\tau} = \frac{U_2^{\tau+\Delta\tau}}{1+\frac{\Delta\tau\pi^2\left(n^2+\left(\frac{m}{a}\right)^2\right)}{R}}$$

and

$$V^{\tau+\Delta\tau} = \frac{V_2^{\tau+\Delta\tau}}{1+\frac{\Delta\tau\pi^2\left(n^2+\left(\frac{m}{a}\right)^2\right)}{R}}.$$

4. LATTICE BOLTZMANN METHODS

The results of the spectral method are compared with those of a couple of lattice Boltzmann methods. Some details of the implementation follow. Further information can be found in Refs. [16–20]. The present applications relies on the lattice Boltzmann equation. For a simulation of the Kolmogoroff flow with Boolean variables lattice Boltzmannes see Ref. [23].

Lattice Boltzmannes are discrete dynamical systems evolving according to a set of cellular automata rules which are both simple and local, in order to make them suitable for massively parallel computation. The molecules of a lattice Boltzmann live in the discrete sites of a (generally regular) lattice tessellating $\Re^n$, and move in a synchronized way along links joining neighboring lattice sites. In this way, molecules moving in different directions can meet at the lattice sites at discrete time intervals, colliding instantaneously according to a definite set of collision rules. The number of molecules and the total momentum are conserved in the collisions at each lattice site. The possibility of using lattice Boltzmannes to simulate hydrodynamical phenomena is based on the conservation,

during the microscopic evolution of the gas, of quantities which can be interpreted as the mass and momentum densities of a fluid. The large scale equations for these densities coincide with the incompressible Navier Stokes equations when the lattice is sufficiently symmetric and the macroscopic velocity of the flow is much smaller than the velocity of the gas particles.

The macroscopic conservation equations were derived in Refs. [16,17] from the underlying microdynamical equation and from the lattice Boltzmann equation. A simplified Boltzmann equation suitable for numerical computation was deduced in Ref. [18] by keeping only those elements of the complete Boltzmann equation necessary to get the first few terms of an Chapman-Enksog multi-scale expansion for small Knudsen and Mach numbers and can be thought of as defining a new dynamical system that shares the properties of space and time discreteness of a lattice Boltzmann, but not its Boolean character. This simplified equation is

$$N_i(\mathbf{x}+\mathbf{c}_i,\tau+1) = N_i(\mathbf{x},\tau) + \Omega_{ij}\left[N_j(\mathbf{x},\tau) - N_j^{\mathrm{eq}}(\mathbf{x},\tau)\right], \tag{19}$$

where Ω_{ij} is the linearized collision operator; $0 \leq N_i \leq 1$, $i = 1,\ldots,b$, are the mean particle populations in the b possible states per lattice site, and $\mathbf{c}_i$ are the corresponding particle velocities. In what follows the two dimensional projected face-centered hypercubic lattice (FCHC) is used, so that $b = 24$. In terms of the local density and velocity of the gas,

$$\rho_0 = N_i \quad \text{and} \quad \rho_0 \mathbf{v} = \mathbf{c}_i N_i, \tag{20}$$

the equilibrium populations N_i^{eq} are

$$N_i^{\mathrm{eq}} = \tfrac{1}{24}(\rho + 2\mathbf{c}_i \cdot \mathbf{v} + 3\mathbf{v} \cdot Q_i \cdot \mathbf{v}),$$

where $Q_{i\alpha\beta} = c_{i\alpha}c_{i\beta} - \frac{1}{2}\delta_{\alpha\beta}$ (the greek indexes mean Cartesian components in $\Re^4$). As shown, the linear operator, Ω denoted by a 24×24 symmetric matrix, acts on the differences between the present and the equilibrium populations corresponding to the local values of ρ and $\mathbf{v}$. The result represents the change of the populations due to collisions. This is added to the N_i and then each updated population is moved to the neighboring site pointed by its respective $\mathbf{c}_i$. The null space of the linearized collision operator determines the quantities conserved during the collisions. Equation (19) is a finite differences equation which can be solved numerically by performing only local operations. Ω_{ij} has five zero eigenvalues associated to the conservation of mass and momentum. An H-theorem exists for Eq. (19) when the non zero eigenvalues are negative and larger than -2, (see Ref. [18]). Under the same conditions, the numerical scheme based on this equation is linearly stable [19].

The Reynolds number attained in a lattice Boltzmann simulation is

$$Re = R^* M L, \tag{21}$$

where L is the size of the lattice referred to the lattice pitch, M is the relation of the characteristic velocity to the lattice Boltzmann velocity ($|\mathbf{c}_i|/2$ for the FCHC lattice),

and R^* is an efficiency factor depending on certain properties of the lattice and of the collision operator, (see Ref. [16]). This factor can be made arbitrarily large by tuning some parameters in the collision operator [18,19], but it is limited by the need of keeping the flow in the collision-dominated regime. The optimum value of R^* to minimize the size of the lattice and the computational work depends on the kind of flow and on the Reynolds number to be attained; see Ref. [20] for a discussion of this issue.

The external force is implemented by increasing the mean populations N_i at each lattice site and time step by small amounts corresponding to an equilibrium distribution function with a velocity equal to the strength of the force per unit mass, see Ref. [6,19].

The method was used for simulating the Kolmogoroff flow at Reynolds numbers 16, 32, 64, and 96, and for several aspect ratios. The initial condition was selected to excite different modes in the range of linear instability for each Reynolds number. The Mach number M was kept smaller than 0.3 in all the cases, to limit the error due to compressibility effects and to the spurious terms in the lattice momentum equation. Regarding compressibility errors introduced by lacking of the Galilean invariance, Kornreich and Scalo [21] have restored this invariance using non linear resonance effects, thus reducing the compressibility errors at supersonic speeds. The evolution was followed for several dozens of residence times. Even though no claim is made that the true final state was attained, a fairly permanent flow resulted in all the simulations, which remained unchanged for several thousands residence times, in the selected cases for which such a long test was conducted.

This (pseudo)-steady state coincides with the one attained with the spectral method, and also with the modified lattice Boltzmann method described below. On the other hand, noticeable differences arise in the transient evolution, which is faster for the lattice Boltzmann than for the real flow. These differences can be attributed to compressibility effects, which are one of the well known shortcoming of lattice Boltzmann methods.

The Mach number should be very small to produce a wide separation between the fast acoustic phenomena and the slow hydrodynamics phenomena of interest, and to keep the spurious terms (of order M relative to the other terms in the momentum equation) below appropriate limits. This, however, is exceedingly expensive in computational terms because the time stepping of the lattice Boltzmann automatically follows the faster time scale, resulting in a very large number of elementary time steps for realistic simulations.

Closer examination of the macroscopic momentum equation arising from the simplified Boltzmann equation (19) [22] shows that the spurious terms are either the gradient of a scalar function or proportional to $\nabla \cdot \mathbf{v}$. The first ones can be accounted for by simply redefining the pressure, and the second ones would vanish if the incompressibility condition $\nabla \cdot \mathbf{v} = 0$ were satisfied. This is what happens for steady flows because the exact continuity equation stemming from (19) is

$$\frac{\partial \rho}{\partial \tau} + \rho \nabla \cdot \mathbf{v}_0 = 0,$$

which explains the good agreement found in the simulations.

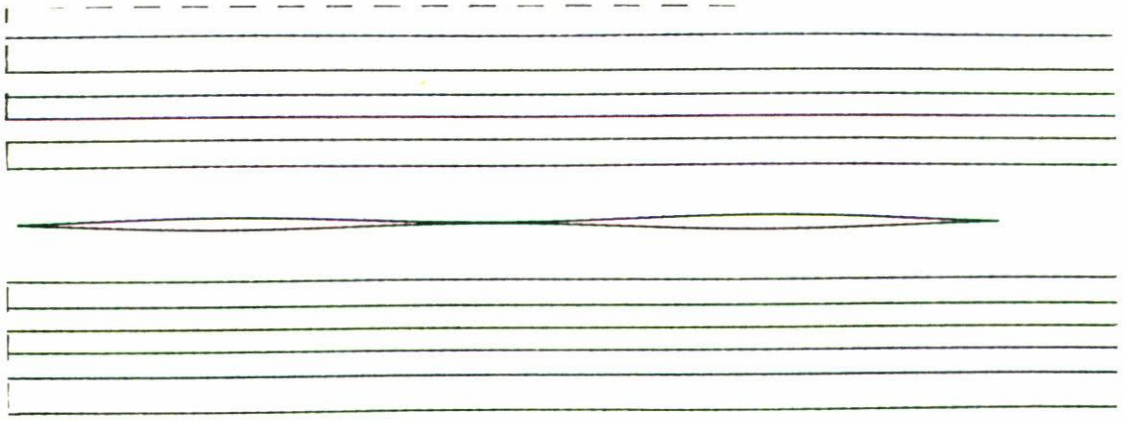

FIGURE 1. Streamlines ($R = 64, a = 3$) for $\tau \ll 1$.

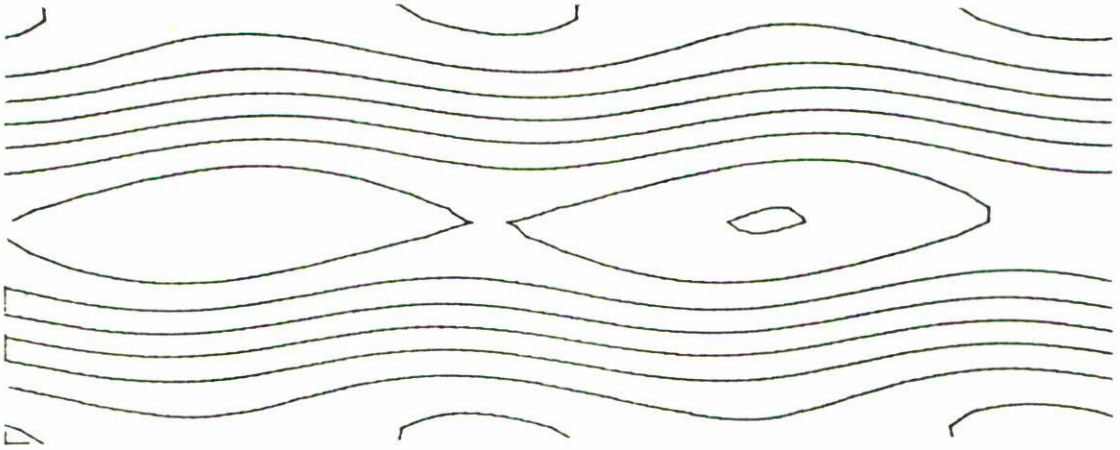

FIGURE 2. Streamlines ($R = 64, a = 3$) for $\tau = O(1)$.

The foregoing observation suggests a cure for the compressibility disease in unsteady lattice Boltzmann flows: it would suffice to modify the treatment of the continuity equation to decrease the actual value of $\nabla \cdot \mathbf{v}$ without necessarily reduce the Mach number. To achieve this goal a time splitting method, similar to the one used with the spectral method, can be used to advantage. First a modified lattice Boltzmann non conserving the number of particles but with constant macroscopic density is set up by modifying the collision operator in Eq. (19), (see Ref. [22]). The momentum equation, which is the only macroscopic equation remaining for this lattice Boltzmann, is appropriate for describing the part of the flow evolution associated to the convection and the viscosity. For the velocity change due to the pressure gradient, which enforces the compressibility condition, a different method is used. In the present case such a method is not of the lattice type but coincides with the second part of the spectral method outlined before. Alternative

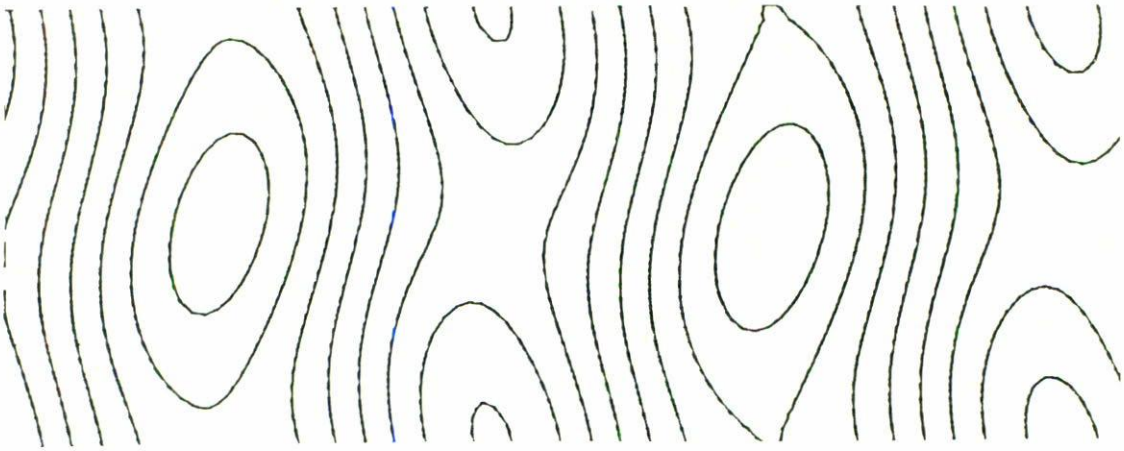

FIGURE 3. Streamlines ($R = 64, a = 3$) for $\tau \gg 1$.

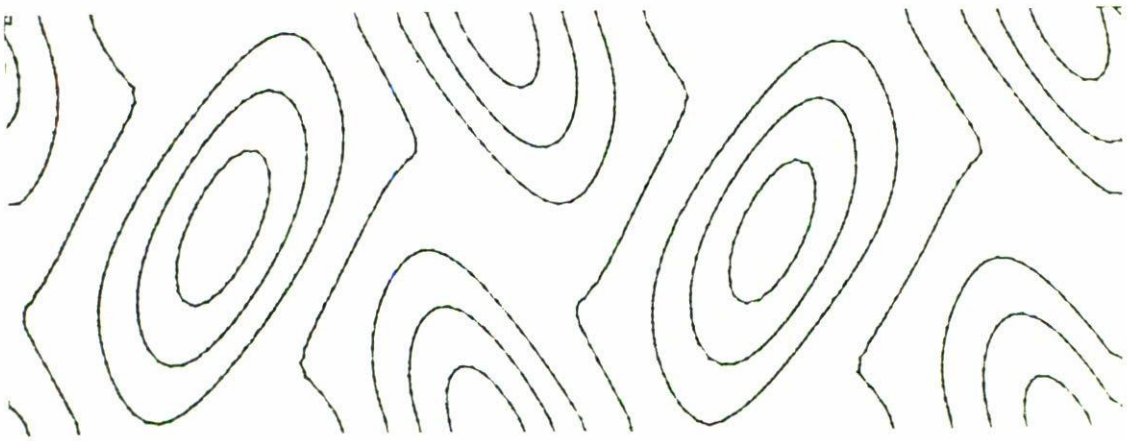

FIGURE 4. Lines of constant vorticity ($R = 64, a = 3$) for $\tau \gg 1$.

treatments within the realm of lattice Boltzmann methods are also possible [22], restoring the locality property.

Actually the results of this hybrid method for the transient period of the Kolmogoroff flow are closer to those of the spectral method that to the ones of the first lattice Boltzmann method, provided that a sufficient number of Fourier modes is used in the computations.

5. NUMERICAL RESULTS

Figures 1 to 4 show the transient non-linear evolution for a Reynolds number of 64, aspect ratio of 3 and an initial perturbation corresponding to an excitation of the fifth harmonic, using the lattice Boltzmann simulation. The body forces act in the horizontal

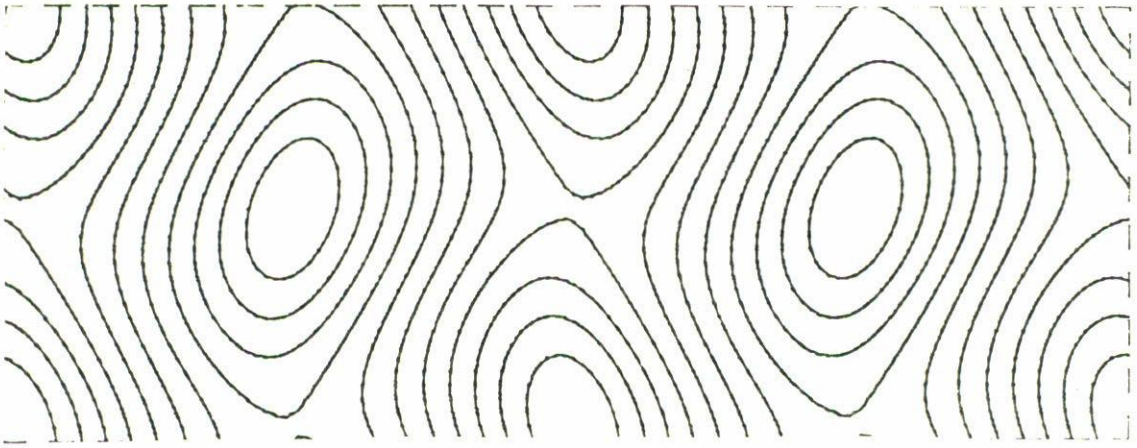

FIGURE 5. Streamlines ($R = 64, a = 4$) for $\tau \gg 1$. Spectral method.

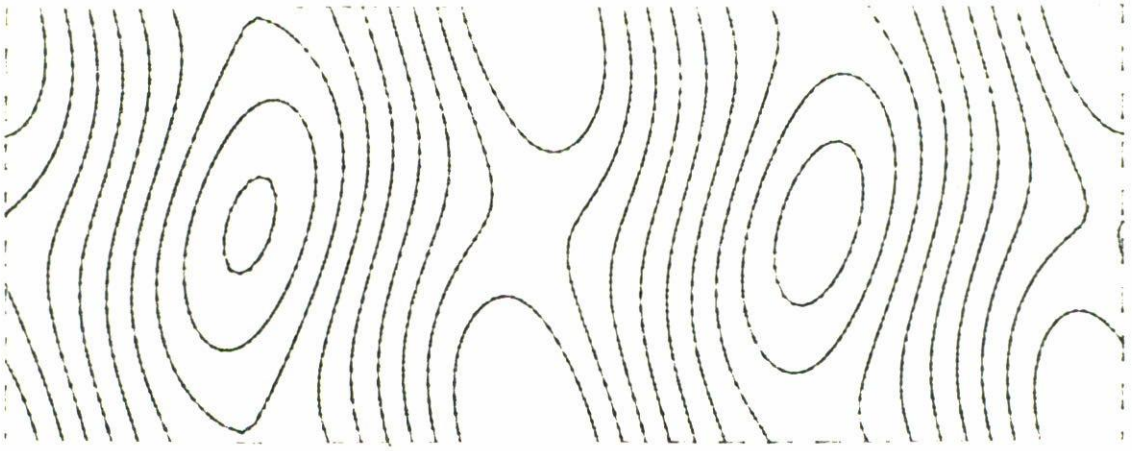

FIGURE 6. Streamlines ($R = 64, a = 4$) for $\tau \gg 1$. Lattice Boltzmann method.

direction being modulated in the vertical direction. It is apparent that the amplitude of the excited mode decreases very fast but due to the relatively large amplitude of the initial perturbation, it excites subharmonics with large amplification rates. Fig. 1 shows the streamline pattern at a time short compared with the residence time. Here, the amplitude of mode 2 has grown producing the typical Kelvin's cat eye structures, with a recirculation zone in the region of maximum shear. These recirculation zones enlarge at later times (of order unity), leading to vortical structures which interact with one another. Finally, at still larger times (Figs. 3 and 4) a pseudo steady-state is attained. This flow which remains unchanged up to times of the order of 10^3 residence times has streamlines that follow mainly the vertical direction. Fig. 4 shows the lines of constant vorticity for the case considered.

Figures 5–7 show the streamline pattern for times larger than the residence time using the three numerical techniques outlined above, that is spectral, lattice Boltzmann and

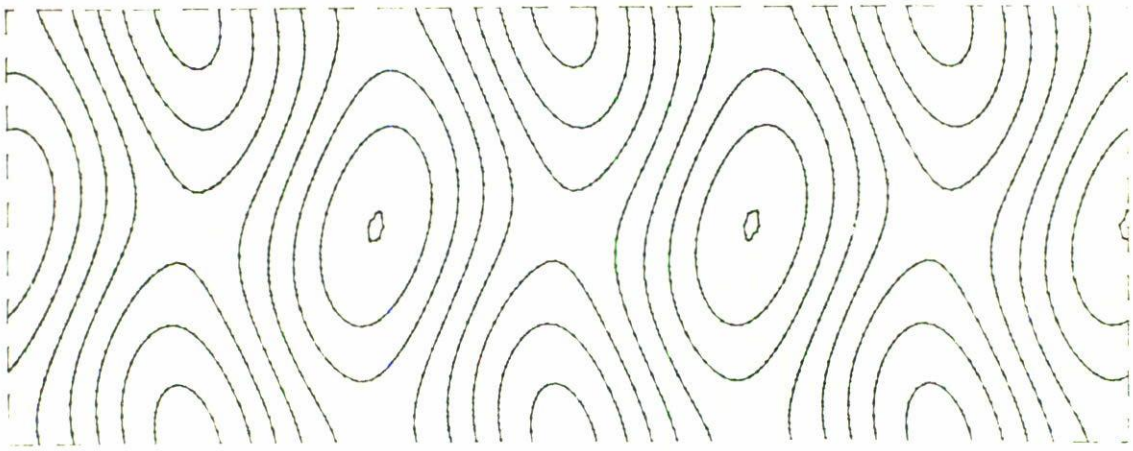

FIGURE 7. Streamlines ($R = 64, a = 4$) for $\tau \gg 1$. Hybrid method.

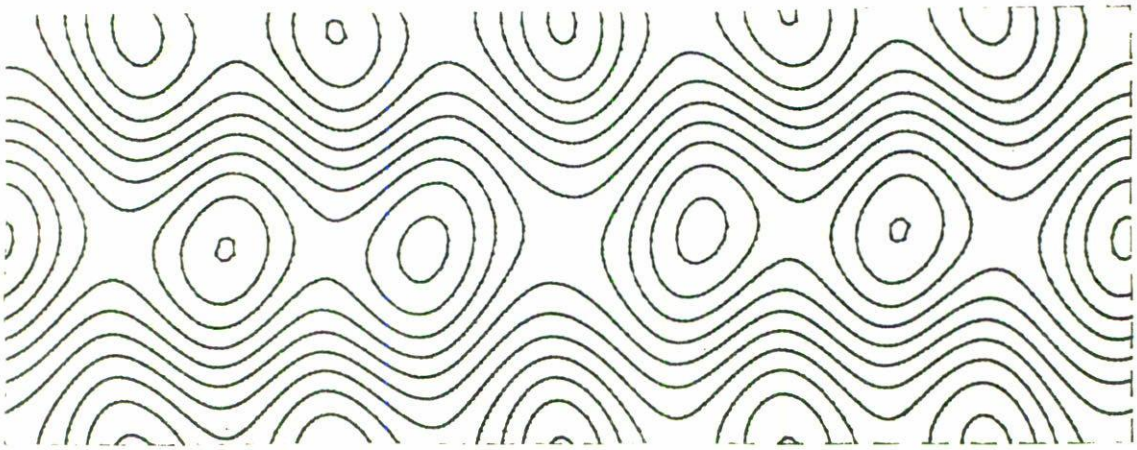

FIGURE 8. Streamlines ($R = 64, a = 6$) for $\tau = 200$. Spectral method.

hybrid, respectively. The Reynolds number used in the calculations was 64, the aspect ratio was $a = 4$ and the initial perturbation to the steady parallel flow was introduced in the second mode. The results of the three methods show very good agreement. Finally, Fig. 8 displays the process of vortex pairing for $R = 64$ and an aspect ratio of 6 obtained with spectral techniques.

ACKNOWLEDGMENTS

This work has been supported by the Instituto de Cooperación con Iberoamérica (Spain) and by the Cray Research Inc. through a research grant on supercomputing. The numerical computations for the spectral method were done on the Cray-YMP at the National University of Mexico (UNAM).

REFERENCES

1. V.I. Arnold and L.D. Meshalkin, *Uspekhi Mat. Nauk* **15** (1960) 247.
2. A.M. Obukhov, *Russ. Math. Survey* **38** (1983) 113.
3. G.I. Sivashinsky and V. Yakhot, *Phys. Fluids* **28** (1985) 1040.
4. L.D. Meshalkin and Ya G. Sinai, *J. Appl. Math. Mech.* (PMM) **25** (1961) 1700.
5. J.S.A. Green, *J. Fluid Mech.* **62** (1974) 273.
6. D.N. Beaumont, *J. Fluid Mech.* **108** (1981) 461.
7. K. Gotoh, M. Yamada and Y.J. Mizishima, *J. Fluid Mech.* **127** (1983) 45.
8. N.F. Bondarenko, M.Z. Gak and F.V. Dolzhansky, *Atmospheric and Ocean Physics* **15** (1979) 711.
9. A. Thess, *Phys. Fluids* **A4** (1992) 1385.
10. G.I. Sivashinsky, *Physica* **D17** (1985) 243.
11. Zh.S. She, *Physics Letters A* **124** (1987) 161.
12. Zh.S. She, Doctoral Thesis, Université de Paris VII (1987).
13. D.O. Martínez, W.H. Matthaeus, S. Chen and D.C. Montgomery, *Phys. Fluids* **6** (1994) 1285.
14. D. Gottlieb and S. Orszag, *Numerical Analysis of Spectral Methods*, SIAM, Philadelphia, USA (1977).
15. M.Y. Canuto, A. Hussaini, Quarteroni and T.A. Zang, *Spectral Methods in Fluid Dynamics*, Springer (1988).
16. U. Frisch, D. d'Humieres, B. Hasslacher, Y. Pomeau and J.P. Rivet, *Complex Systems* **1** (1987) 646.
17. S. Wolfram, *J. Stat. Phys.* **45** (1986) 471.
18. F.J. Higuera and J. Jiménez, *Europhysics Lett.* **9** (1989) 663.
19. F.J. Higuera, S. Succi and R. Benzi, *Europhysics Lett.* **9** (1989) 345.
20. F.J. Higuera and S. Succi, *Proceedings of the 5th Int. Symposium on Num. Met. in Engng.* Springer, (1989) 273.
21. P.J. Kornreich and J. Scalo, *Physica* **D 69** (1993) 333.
22. F.J. Higuera, in *Numerical Methods for Simulation of Complex Flows* (1992) 49.
23. R. Benzi and S. Succi, *J. Stat. Phys.* **56** (1989) 69.